Triboelectric Nanogenerator Built on Suspended 3D Spiral Structure as Vibration and Positioning Sensor and Wave Energy Harvester

Youfan Hu,[†,⊥] Jin Yang,[†,‡,⊥] Qingshen Jing,[†] Simiao Niu,[†] Wenzhuo Wu,[†] and Zhong Lin Wang[†,§,*]

[†]School of Material Science and Engineering, Georgia Institute of Technology, Atlanta, Georgia 30332-0245, United States, [‡]Department of Optoelectronic Engineering, Chongqing University, Chongqing 400044, People's Republic of China, and [§]Beijing Institute of Nanoenergy and Nanosystems, Chinese Academy of Sciences, Beijing 100083, People's Republic of China. [⊥]Y. Hu and J. Yang contributed equally to this work.

ABSTRACT An unstable mechanical structure that can self-balance when perturbed is a superior choice for vibration energy harvesting and vibration detection. In this work, a suspended 3D spiral structure is integrated with a triboelectric nanogenerator (TENG) for energy harvesting and sensor applications. The newly designed vertical contact–separation mode TENG has a wide working bandwidth of 30 Hz in low-frequency range with a maximum output power density of 2.76 W/m^2 on a load of 6 MΩ. The position of an in-plane vibration source was identified by placing TENGs at multiple positions as multichannel, self-powered active sensors, and the location of the vibration source was determined with an error less than 6%. The magnitude of the vibration is also measured by the output voltage and current signal of the TENG. By integrating the TENG inside a buoy ball, wave energy harvesting at water surface has been demonstrated and used for lighting illumination light, which shows great potential applications in marine science and environmental/infrastructure monitoring.

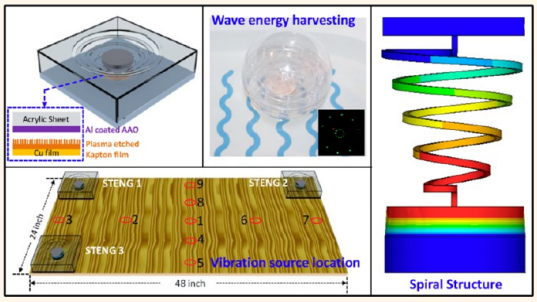

KEYWORDS: triboelectric nanogenerator · 3D spiral structure · buoy ball · self-powered sensor

Vibrations are common mechanical phenomena that can be found in ambient environment, such as the vibration motions of engines, vibrations in buildings and bridges, the shaking of a flying aircraft, and ocean wave oscillations. In many cases, antivibration technology is required in order to stabilize the structure and reduce noises. Various transducers have been fabricated for monitoring and detecting vibrations and impacts. On the other hand, vibration is a source of energy. Generally, there are three ways to convert vibration into electric energy, namely, by using electromagnetic,[1,2] electrostatic,[3,4] and piezoelectric effects.[5−9] Most recently, we have invented a new approach, the triboelectric nanogenerator (TENG), for harvesting ambient mechanical energy based on the coupling of the triboelectric effect and electrostatic induction.[10−14] The periodic contact and separation between two materials with opposite triboelectric polarities alternatingly drives the induced electrons to flow between electrodes through an external circuit. It is a cost-effective, simple, and robust technique for energy harvesting. Alternatively, a TENG can serve as an active sensor for sensing mechanical vibration/triggering using the electric output by itself without a driving power source. A mechanical structure positioned at its critical state of mechanical equilibrium is unstable and very sensitive to the disturbance in the environment. If such a structure can balance itself when disturbed and oscillate around the equilibrium point, it can be superior for vibration energy harvesting and impact detection at a weak ambient vibration. The 3D spiral structure is a typical example. It is a three-dimensional curve around an axis at a continuously reducing radius while moving parallel to the axis, which can be simply regarded as a conical-shaped spring structure. Loaded with a seismic mass, the suspended 3D spiral

* Address correspondence to zlwang@gatech.edu.

Received for review October 6, 2013 and accepted October 29, 2013.

Published online October 29, 2013
10.1021/nn405209u

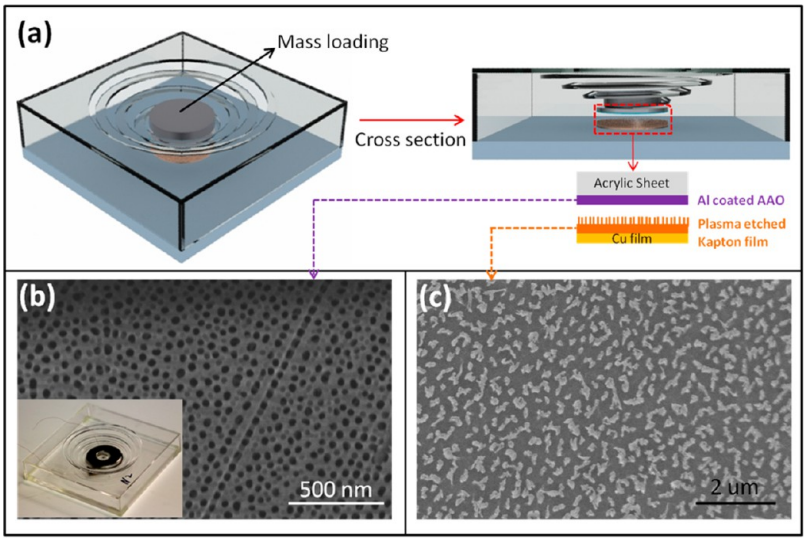

Figure 1. Triboelectric nanogenerator built on a suspended 3D spiral structure. (a) Schematic diagram of the device and its cross section view. SEM image of the surface morphology of (b) aluminum and (c) the Kapton film. The inset of (b) is a photo of the real device.

structure oscillates in response to external disturbance at a high sensitivity.

In this work, a TENG that operates in the vertical contact−separation mode was built at the front of the seismic mass in a spiral structure. The spiral structure behaves like a spring in response to an external disturbance. The TENG built on the spiral structure (spiral TENG) shows a wide working bandwidth of 30 Hz in the low-frequency range, and a maximum output power density of 2.76W/m^2 was achieved on a load of 6 MΩ. Furthermore, by using three spiral TENGs (STENGs) to construct a multichannel vibration active sensor system, the location of an in-plane vibration source was positioned within an error of <6% without supplying an external power source. Furthermore, by positioning the STENG inside a fully closed buoy ball, we demonstrated that the structure can be used to harvest the vibration energy from the wavy water surface, which is strong enough to drive 20 LED lights. Our study establishes a newly designed STENG that is well suited not only as a self-powered positioning or vibration sensor but also for harvesting wave energy in ambient environment such as in wind, river water, and the ocean.

RESULTS AND DISCUSSION

A schematic diagram of the STENG with a vertical contact−separation mode is shown in Figure 1a. Due to the suitable strength, light weight, easy processing, and low cost, an acrylic sheet is chosen as the structural material. The detailed fabrication process is described in the Methods section. The working parts that generate the electricity are two round plates facing each other, which is marked in Figure 1a with a red dashed line. One is attached at the bottom of the 3D spiral structure. The other one is centered and fixed on the upper surface of the cube's bottom. The height of the cube was adjusted to have these two plates be in slight contact when the spiral is relaxed and in equilibrium. The upper contact surface is an aluminum film coated on an anodic aluminum oxide (AAO) template. Figure 1b is a scanning electron microscopy (SEM) image of the aluminum surface. There are nanopores uniformly distributed on the surface with an average diameter of 30 nm, which are able to increase the effective contact area for triboelectrification. The lower contact surface is a Kapton film. The surface of the Kapton film was modified to introduce aligned nanowire structures. Figure 1c is an SEM image of the obtained surface. The uniformly distributed nanowire features can further increase the surface roughness and the effective surface area of the STENG for effective triboelectrification.

Figure 2 sketches the electricity generation mechanism of the STENG. It can be explained by the coupling between the triboelectric effect and electrostatic induction. When the STENG is working, the spiral oscillates in response to an external mechanical disturbance, and the distance $x(t)$ between the Al and Kapton film changes, as shown in Figure 2a. In the original state, when there is no mechanical disturbance, the spiral is relaxed, and the two round plates slightly contact each other (Figure 2b). According to the triboelectric series,[15] in which materials are listed in order of the polarity of charge separation when they are touched with another object, electrons are transferred from the Al film to the Kapton film, resulting in positive and negative triboelectric charges on the Al and Kapton surface, respectively. When the cube structure experiences a mechanical disturbance, the spiral starts to oscillate along the vertical direction. As the spiral contracts, the contacted surfaces separate

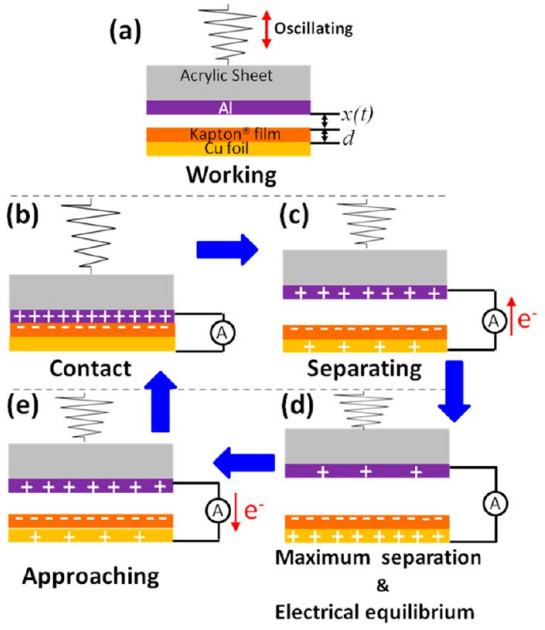

Figure 2. Working mechanism of the STENG. (a) Schematic diagram showing a STENG in working status. The spiral is oscillating, and the distance between the two contact surfaces $x(t)$ is changing. (b–e) Full cycle of the electricity generation process.

(Figure 2c). Because the Al electrode has a higher potential than the Cu electrode beneath the Kapton film, electrons flow from the Cu electrode to the Al electrode through the external circuit to neutralize the positive triboelectric charges in the Al electrode. The flow of electrons lasts until the separation is maximized, and an electrostatic equilibrium is reached (Figure 2d). Then the spiral starts to release to the original equilibrium position, and the two plates approach each other. Thus, the former electrostatic equilibrium is broken. Electrons flow back from the Al electrode to the Cu electrode through the external circuit (Figure 2e). Finally, when these two plates contact each other again, there is no current flow in the external circuit, and the triboelectric charge distribution is restored to the original status (Figure 2b). This is a full cycle of the electricity generation process. As the spiral oscillates in response to the mechanical disturbance in the environment, electricity is generated.

In principle, the STENG can be regarded as two flat-panel capacitors connected in series. We assume the charge on the Al film is Q_1, the charge on the Kapton film is Q, and the charge on the Cu foil is Q_2. The corresponding charge densities are σ_1, σ, and σ_2. S is the area of the round plate. ε_0 is the dielectric constant of the vacuum, and ε_r is the relative dielectric constant of the Kapton film. The thickness of the Kapton film is d, and the distance between the Al film and the Kapton film $x(t)$ changes as the spiral oscillates. On the basis of electrostatic induction and conservation of charges, $Q_1 + Q_2 = -Q$. The open circuit voltage V_{oc} and short circuit current I_{sc} can be expressed as[16]

$$V_{oc} = -\frac{\sigma x(t)}{\varepsilon_0} \quad (1)$$

$$I_{sc} = \frac{-S\sigma d}{\varepsilon_r\left(\frac{d}{\varepsilon_r} + x(t)\right)^2}\frac{dx(t)}{dt} \quad (2)$$

We can see that V_{oc} is proportional to the distance between the two plates. It reaches a maximum when the two plates are furthest separated. Also V_{oc} is proportional to the triboelectric charges generated on the contacting surface, which depends on the property of the two surfaces and the friction process. It can be enhanced by choosing proper materials and modified surface morphology, as we have done in this work. By checking eq 2, we can conclude that the output current is proportional to the distance change rate of the two plates, which is determined by the spiral's oscillation, and also proportional to the generated triboelectric charges.

For such a suspended structure, the frequency response is of great interest for the output performance. A vibration-impacting model was used to analyze the frequency characteristics of the STENG, as shown in Figure 3a. The 3D spiral structure with seismic mass load at the bottom is modeled as a movable mass m suspended by a spring k_z and a damper c_z. When an external disturbance is experienced by the cube, the bottom of the cube makes a displacement of Z_2, which causes the seismic mass to vibrate relative to the bottom of the cube with a displacement of Z_1. The motions and their interrelationship can be described by a differential equation as[17]

$$\ddot{Z}_r + 2\xi_z\dot{Z}_r + Z_r = \left(\frac{\omega}{\omega_0}\right)^2 \sin(\rho\pi) + f(Z_r, \dot{Z}_r) \quad (3)$$

$$f(Z_r, \dot{Z}_r) = \begin{cases} 0 & (Z_r > 0) \\ -2\frac{\omega}{\omega_{0z}}\xi_z\dot{Z}_r - \left(\frac{\omega}{\omega_0}\right)^2 Z_r & (Z_r < 0) \end{cases} \quad (4)$$

where $Z_r = (Z_1 - Z_2)/U_z$, and $Z_2 = U_z \sin(\omega t)$. U_z is the amplitude of the external disturbance. $\ddot{Z}_r$ and $\dot{Z}_r$ are the relative acceleration and velocity of the mass with respect to the cube's bottom. ξ_z is the primary suspension damping characteristic and is defined as $\xi_z = c_z/(2m\omega_0)$. ω is the excitation frequency, and $\omega_0 = (k_z/m)^{1/2}$. We can see that a nonlinear function $f(Z_r, \dot{Z}_r)$ is introduced into the motion model, which is induced by the impact between the two contacting surfaces. This will lead to a different frequency response compared to the general linear model.

On the basis of eq 3, a finite element analysis was carried out to simulate the mechanical behavior of the STENG under an external disturbance. Young's

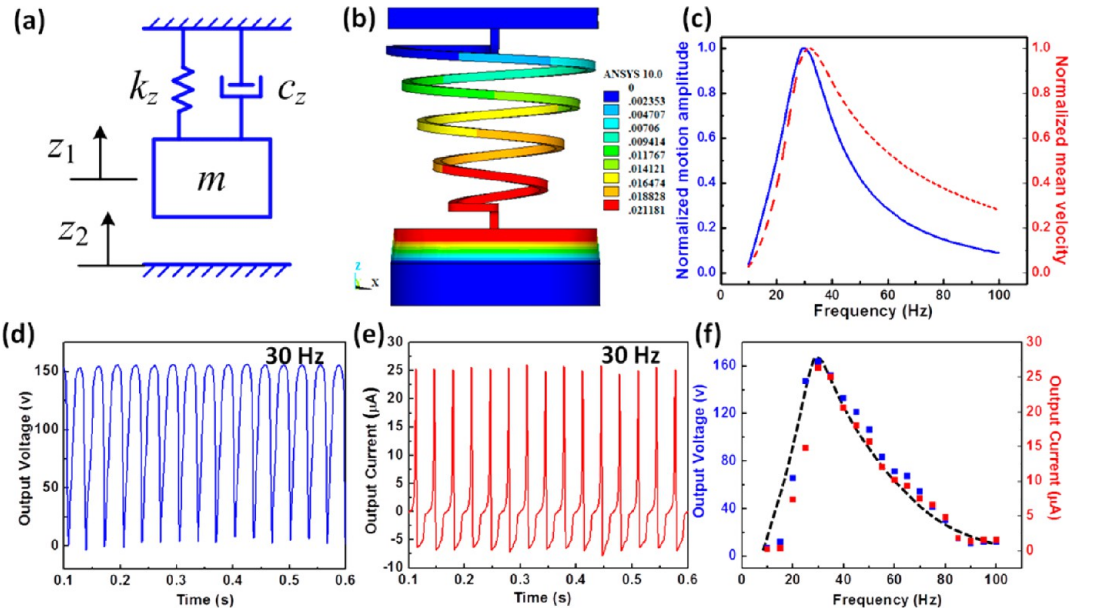

Figure 3. Simulation and output performance of the STENG. (a) Vibration-impacting model for simulating the frequency response of the STENG. (b) Instant motion state result of the vertical contact−separation mode by ANSYS. (c) Simulated frequency response of the STENG and corresponding mean velocity of the seismic mass. (d) Output voltage and (e) output current of the STENG at the resonant frequency of 30 Hz. (f) Measured frequency response of the STENG.

modulus and Poisson's ratio of the spring are chosen to be 2 GPa and 0.6, respectively. Figure 3b shows an instant motion state when the two round plates are separated from each other due to the contraction of the spiral under an external disturbance. The frequency response of the STENG is shown as the blue line in Figure 3c. The resonant frequency of the system is 30 Hz. Due to the vibration-impacting motion of the two surfaces, a nonlinear behavior appears in the frequency response, resulting in an asymmetric spectrum and a broad working bandwidth of about 30 Hz. The performance of the real device was tested by putting the STENG on an electrodynamic shaker, which works as an external vibration source generating a sinusoidal output with controlled amplitude and acceleration along the vertical direction. The vibration frequency is in a range from 10 to 100 Hz with an increasing step of 5 Hz. Figure 3d and e are the open-circuit voltage and short-circuit current under a vibration frequency of 30 Hz. The open-circuit voltage reaches 150 V, and the short-circuit current is around 27 μA, corresponding to a current density of 20 mA/m^2. The frequency response of the STENG's output performance is shown in Figure 3f. Both the voltage and current present a rapid increase with an increase of frequency from 10 to 30 Hz. Then, both of them gradually dropped to their minima as the frequency increases from 30 to 100 Hz. Also, we compared the integral area size of the current peak under different frequencies. It corresponds to the transferred charges between the two electrodes through the external circuits, which are proportional to the generated triboelectric charges.[16] It reaches a maximum at 30 Hz as well. As the simulation results show in Figure 3c, the spiral resonates at 30 Hz with the largest motion amplitude, which makes the separation distance between the two plates reach a maximum and causes a larger impact when the two plates contact each other. The latter contributes to the increased contact surface and the enhanced triboelectric charge generation. Because I_{sc} is proportional to the distance change rate of the two plates, we plot the normalized mean velocity of the seismic mass as the red dashed line in Figure 3c. The maximum is located at 32 Hz, which is just slightly shifted from the resonant frequency of 30 Hz. On the basis of all the facts we stated above and according to eqs 1 and 2, we obtained both the maximum V_{oc} and I_{sc} when the spiral is resonanting.

The power output capability of the STENG was investigated at the resonance frequency by using resistors as external loads. As shown in Figure 4a, the output voltage increases quickly as the resistance increases from 10 Ω to 40 MΩ, and then saturates when the resistance is further increased. The output current follows a reverse trend compared to the output voltage. As a result, the output power density is maximized at 2.76 W/m^2 with a load resistance of 6 MΩ, which is shown in Figure 4b.

STENGs can serve as self-powered active sensors in passive mode for vibration detection and monitoring. This means that whenever there is a vibration disturbance in the environment experienced by the STENG, the STENG will be triggered to generate an indicating electric signal. As in some situations vibrations are undesirable and harmful, in addition to vibration

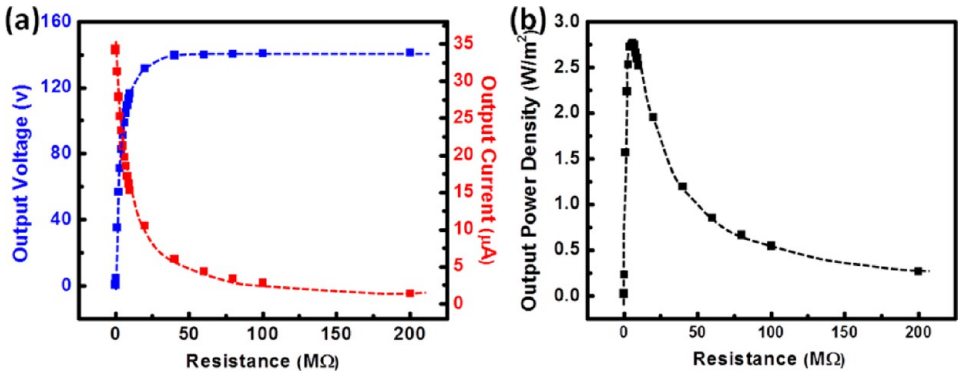

Figure 4. Output performance of the STENG with external load. (a) Dependence of the output voltage and current on the external load resistance. (b) Dependence of the output power density on the resistance of the external load, indicating a maximum power output when R = 6 MΩ.

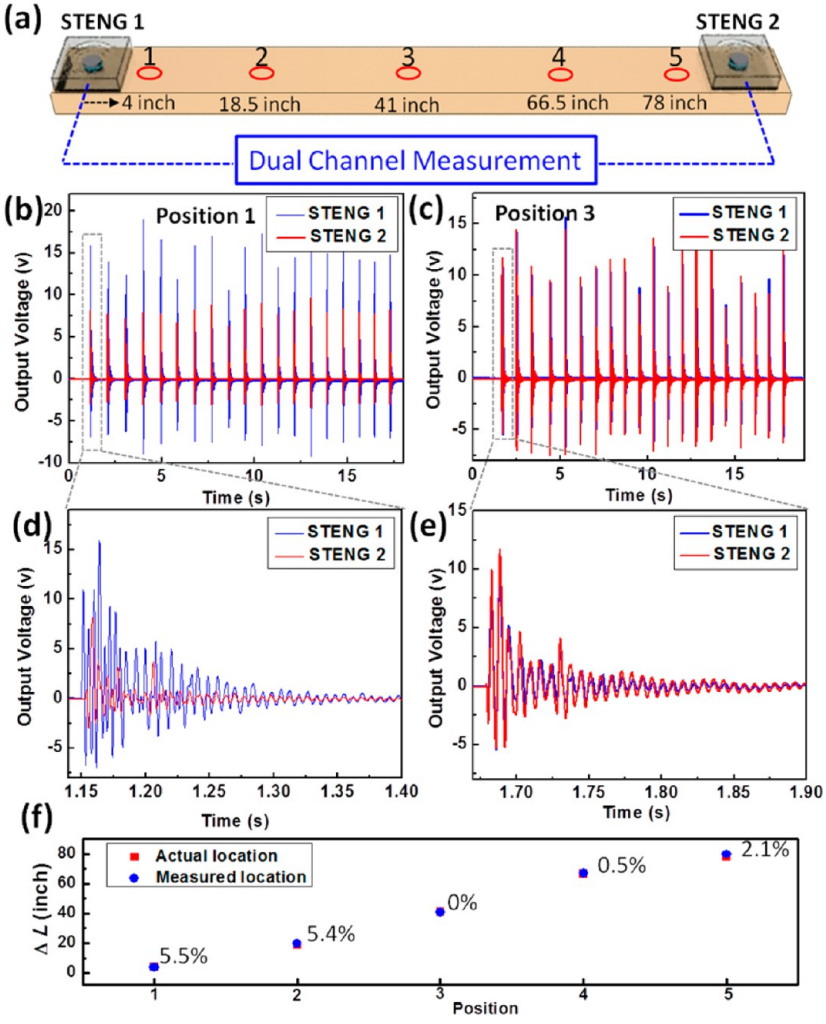

Figure 5. Vibration source location in one dimension. (a) Schematic diagram of experimental setup shows two STENGs that are respectively positioned at the two ends of a board. (b) Recorded signal patterns when the impact is located at position 1. (c) Recorded signal patterns when the impact is located at position 3. (d) Enlarged view of one peak signal in (b). (e) Enlarged view of one peak signal in (c). (f) Comparison of the measured location and actual location of the vibration source location and corresponding location error.

detection, the vibration source positioning is very important and of great practical value. Here we used STENGs to construct a multichannel active sensor system, and the in-plane vibration source positioning was realized. Figure 5a shows the demonstration of the vibration source location on a wood board with dimensions of 2 in. × 4 in. × 84 in. Two STENGs were put on the two ends of the lumber and could collect signal

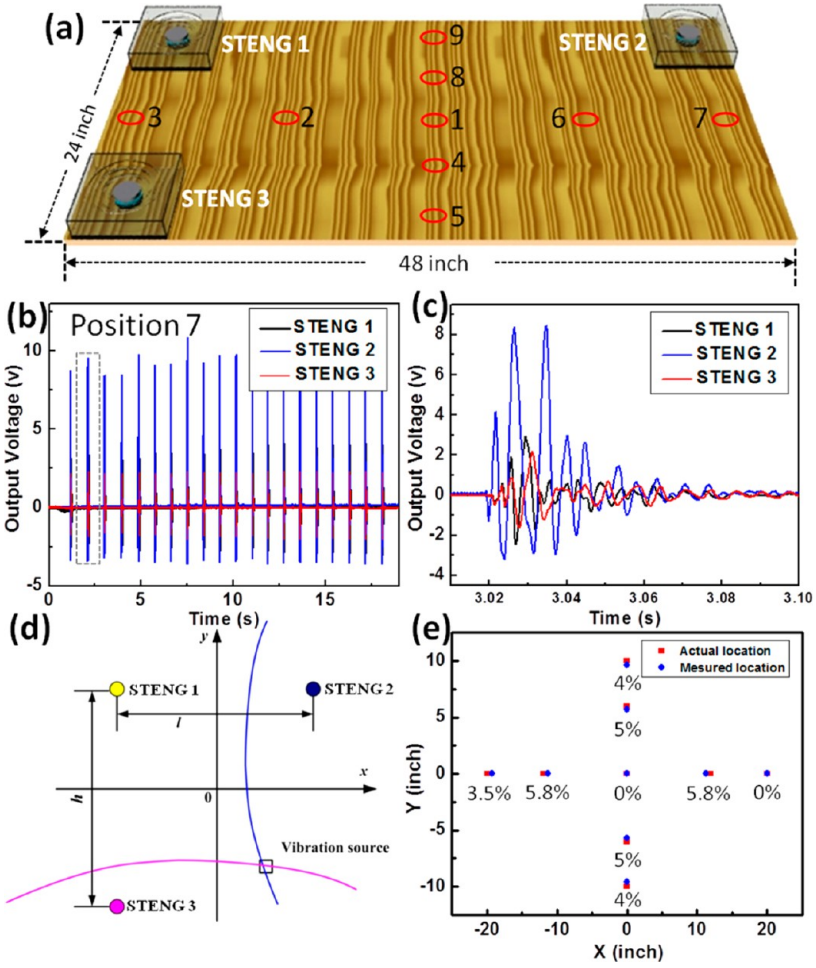

Figure 6. Vibration source location on a wood board. (a) Schematic diagram of the experimental setup shows three STENGs positioned at the three corners of a wood board. (b) Recorded signal patterns when the impact is located at position 7. (c) Enlarged view of one peak signal in (b), which is indicated by a dashed gray rectangle. (d) Schematic diagram of the principle to locate the vibration source. (e) Comparison of the measured location and actual location of the vibration source and corresponding location error.

simultaneously by using a customized LabVIEW (National Instruments) code for dual-channel data acquisition. A small hammer was used to gently hit different positions on the board periodically. The locations of the impact were indicated with red circles and are numbered as shown in Figure 5a. Figure 5b and c are two typical recorded signal patterns when the impacts are located at position 1 and position 3, respectively. First, when the impact is located at position 1, as STENG 1 is closer to the vibration source, the recorded signal level from STENG 1 is obviously larger than the one coming from STENG 2. When the impact is located at position 3, which is the center position between STENG 1 and STENG 2, the signals received from these two STENGs are almost at the same level. Figure 5d and e are the corresponding enlarged view of one signal peak in Figure 5b and c, respectively. We can see that when the vibration propagates to the STENGs, electric signals are generated and then are gradually damped. For the case of position 1, the vibration first arrived at STENG 1; thus the arrival time of the first signal peak observed in STENG 1 is earlier than that from STENG 2. If the distance between these two STENGs is fixed, and we determine the vibration propagation velocity and the time difference of arrival, then we can locate the position of the vibration source between these two STENGs. Figure 5f shows the experimental results. The blue dots represent the measured location of the vibration source's position, and the red cube indicates the actual location for comparison. If the actual location of the vibration source is at (x_0, y_0) and the measured location is at (x, y), we define the location error as $E_{location} = |[(x - x_0)^2 + (y - y_0)^2]^{1/2}|$. For a board with a length of 84 in., the location error is less than 5.5%, and the most accurate positioning point is at the center without error. The error is greatly limited by the sampling rate of our data acquisition equipment, which currently is 4000, corresponding to a time resolution of 0.25 ms. For a longer board, as the time difference of arrival will be more distinct, the spatial resolution is expected to be much better than this.

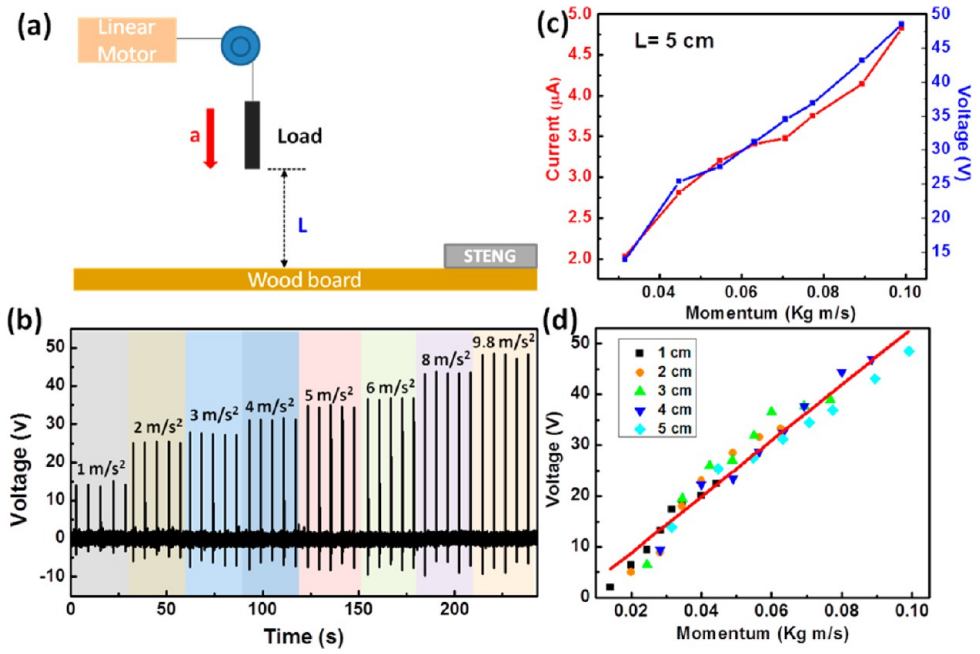

Figure 7. Self-powered dynamic sensor. (a) Schematic diagram of the experimental setup. (b) Recorded voltage signal when the mass is released from L = 5 cm at different accelerations. (c) Measured voltage/current signals with different mass load momentum at L = 5 cm. (d) Comparison of measured voltage signals under different testing conditions. A linear relationship is revealed.

Then the vibration source positioning test was carried out on a wood board with dimensions of 1 in. × 24 in. × 48 in. Three STENGs were positioned on three corners of the board, as shown in Figure 6a. A three-channel measurement was applied to acquire data from these three STENGs simultaneously. Nine different positions on the board were checked, as indicated by the red circles in Figure 6a. A representative signal pattern is shown in Figure 6b, which was acquired when the small hammer hit position 7. Because STENG 2 is the closest one to the vibration source, it obtains the highest signal level. For STENG 1 and STENG 3, the signal levels are similar due to the equal distance from the vibration source. Figure 6c is the enlarged view of one signal peak in Figure 6b, which is indicated by a dashed gray rectangle. The vibration propagated and first arrived at STENG 2 and then arrived at STENG 1 and STENG 3 at the same time. Thus the first signal peak from STENG 2 is earlier than the two coming from STENG 1 and STENG 3. The principle to locate the vibration source is depicted in Figure 6d. We can obtain the arrival time differences of the signal among the three STENGs. Combining the vibration propagation speed, we can get information on the distance difference from the vibration source to STENG 1 and STENG 2 (D_1), as well as the distance difference from the vibration source to STENG 1 and STENG 3 (D_2). The track of an object that maintains the same distance difference from two fixed points is a hyperbolic curve, as indicated by the blue and purple curves in Figure 6d. The vibration source is located at the intersection of the two hyperbolic curves by solving the equations

$$\begin{cases} \dfrac{x^2}{\left(\frac{D_1}{2}\right)^2} - \dfrac{\left(y+\frac{h}{2}\right)^2}{\left(\frac{l}{2}\right)^2 - \left(\frac{D_1}{2}\right)^2} = 1 \\ \dfrac{y^2}{\left(\frac{D_2}{2}\right)^2} - \dfrac{\left(x-\frac{l}{2}\right)^2}{\left(\frac{h}{2}\right)^2 - \left(\frac{D_2}{2}\right)^2} = 1 \end{cases} \quad (5)$$

in which l is the distance between STENG 1 and STENG 2, and h is the distance between STENG 1 and STENG 3. The corresponding experimental results are shown in Figure 6e. The position at the center of the board is accurately located without error, and the location error for other positions is less than 5.8%.

According to eqs 1 and 2, the output signal of STENG is sensitive to the dynamic process of the experienced mechanical disturbance. So it can work as a dynamic sensor to realize real-time vibration monitoring. Figure 7a shows the experiment setup to demonstrate this characterization. A STENG is fixed on the edge of a wood board. A mass load of 100 g is hung at a horizontal distance of 10 in. away from the STENG. The movement of the mass in the vertical direction is controlled by a linear motor through a pulley. The mass is released from a series of vertical heights (L = 1, 2, 3, 4, and 5 cm) with different acceleration (a = 1, 2, 3, 4, 5, 6, 8, and 9.8 m/s^2) to hit the wood board. Figure 7b shows the experimental results when L = 5 cm.

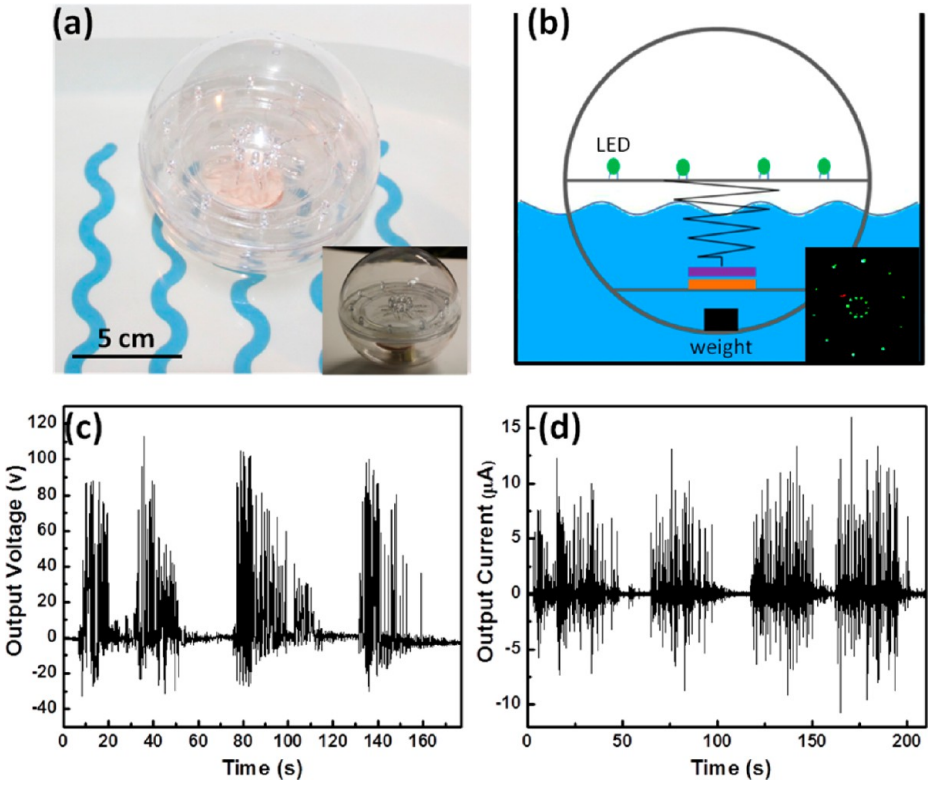

Figure 8. Demonstration of wave energy harvesting. (a) Photo of the real device placed in a basin filled with water to simulate a buoy floating in an ocean/river. LED lights are installed on the upper acrylic plate. (b) Schematic cross section view of (a). The inset is a recorded top view image of the lighted buoy when powered by water waves. (c) Output voltage and (d) output current of the STENG integrated in a buoy when there is a slight disturbance in the water.

As the acceleration increases, the measured voltage signal increases. For a fixed travel distance, a larger acceleration means a larger velocity at the destination, and thus a larger momentum of the impact. Figure 7c shows that there is a linear relationship between the measured voltage/current signals and the mass load's momentum when it hits the wood board's surface. We summarized all the results of different experimental conditions in Figure 7d, including the load mass falls from five different vertical heights with eight different accelerations. All of the data follow a linear relationship between the output signal and the load mass's momentum. In this case, our STENG works as an active dynamic sensor for impact momentum sensing and monitoring.

As for ocean waves, due to the huge power of the wave motion, which can easily achieve 50 kW per meter of wavefront at the most energetic locations,[18] harvesting mechanical energy from ocean wave oscillations to electrical energy has long been pursued as an alternative or sustainable power source.[19−21] The principal barrier to harvesting this power is the very low and varying frequency of ocean waves. A buoy is a floating device commonly used on rivers or seas that is allowed to drift and sway with the waves. It can be used for many purposes, including mooring, life saving, weather monitoring, and, the most general one, as a sea mark. As the buoy sways with the waves, it is possible that we can integrate STENGs with a buoy to harvest wave energy for powering lights. Figure 8a is an image of the real device that was placed in a basin filled with water to simulate the actual working conditions in the ocean. The cross section view is sketched in Figure 8b. The detailed integration process is described in the Methods section. Figure 8c and d are the output performance of the STENG when it is integrated in the buoy. When there is a slight disturbance in the water, the measured output voltage of the STENG reaches 110 V, and the measured output current can exceed 15 μA. Then 20 LEDs were integrated on the upper acrylic to demonstrate a self-powered lighted sea mark, as shown in the inset of Figure 8b and the video in the Supporting Information. This is just the first step toward utilizing wave energy by a STENG. Considering the good performance, if we integrate more functions onto the buoy, such as monitoring sensors for air temperature, barometric pressure, wind speed, and direction, and linked it to meteorological centers through satellite networks, it could be used for forecasting, climate study, and more. Such a self-powered sensor network can be a key technology for many applications of this type.

CONCLUSIONS

In conclusion, a suspended 3D spiral structure was used to construct a TENG in the vertical

contact−separation mode. This unstable mechanical structure can balance itself when perturbed, which makes it a superior choice for vibration energy harvesting and vibration detection. The newly designed STENG works in the low-frequency range with a wide working bandwidth of 30 Hz. The maximum output power density of 2.76 W/m^2 on a load of 6 MΩ is achieved at a resonant frequency of 30 Hz. Using three STENGs, the position of an in-plane vibration source is located with an error less than 6%. Such an error can be improved by increasing the sampling rate of the data acquisition equipment. By integrating the STENG with a buoy ball, self-powered lighted sea mark were demonstrated using the energy harvested from water waves. Such a STENG has potential applications in marine science, environmental sciences, and more.

METHODS

Fabrication of the STENG. The STENG was constructed with an acrylic sheet. First, a 2D spiral structure with an outside diameter of 2.8 in. was cultured on the center of a 4 in. × 4 in. square acrylic sheet. After loading with a seismic mass, and released from the plane, a suspended 3D spiral structure was achieved. Then, a cube was constructed by using it as the upper surface. The working parts to get the electricity generation are two round plates facing each other. One of them is a round acrylic substrate covered with AAO template, which was attached at the bottom of the 3D spiral structure. A thin layer of aluminum was coated on the AAO template to work both as an electrode and as one of the contact surfaces. Another round plate is a Kapton film covered with Cu foil, which was centered and fixed on the upper surface of the cube's bottom. The Cu foil works as the other electrode, and the Kapton film works as the other contact surface. The height of the cube was adjusted to cause these two plates be in slight contact when the spiral is relaxed and in equilibrium. The surface of the Kapton film was dry-etched by using inductively coupled plasma (ICP) to create aligned nanowire structures.

Integration of the STENG with a Buoy. The buoy is a transparent acrylic hollow ball with a diameter of 14 cm. A weight was loaded at the bottom to make it float in the water. One round acrylic plate with a suspended 3D spiral structure on it was stuck on the center of the ball. Another round acrylic plate with a smaller diameter was stuck on the lower part of the ball. The working parts to generate electricity are the same as in the previous section. The distance of the two acrylic plates is adjusted to make the surfaces of the Al-coated AAO film and the plasma-etched Kapton film just contact each other when the spiral is relaxed. To demonstrate the application of a self-powered lighted sea mark, 20 LEDs were integrated on the upper acrylic plate and serially connected with the STENG.

Conflict of Interest: The authors declare no competing financial interest.

Supporting Information Available: A video recorded for wave energy harvesting demonstration is included. This material is available free of charge *via* the Internet at http://pubs.acs.org.

Acknowledgment. Research was supported by Basic Energy Sciences DOE, MURI from Airforce, the Knowledge Innovation Program of the Chinese Academy of Sciences (KJCX2-YW-M13), and the "Thousands Talents" Program for a pioneer researcher and his innovation team, China.

REFERENCES AND NOTES

1. Amirtharajah, R.; Chandrakasan, A. P. Self-Powered Signal Processing Using Vibration-Based Power Generation. *IEEE J. Solid-State Circ.* **1998**, *33*, 687–695.
2. Williams, C. B.; Yates, R. B. Analysis of a Micro-Electric Generator for Microsystems. *Sens. Actuators, A* **1996**, *52*, 8–11.
3. Meninger, S.; Mur-Miranda, J. O.; Amirtharajah, R.; Chandrakasan, A. P.; Lang, J. H. Vibration-to-Electric Energy Conversion. *IEEE Trans. VLSI Syst.* **2001**, *9*, 64–76.
4. Roundy, S.; Wright, P. K.; Rabaey, J. A Study of Low Level Vibrations as a Power Source for Wireless Sensor Nodes. *Comput. Commun.* **2003**, *26*, 1131–1144.
5. Glynne-Jones, P.; Beeby, S. P.; White, N. M. Towards a Piezoelectric Vibration-Powered Microgenerator. *IEE Proc.: Sci. Meas. Tech.* **2001**, *148*, 68–72.
6. Roundy, S.; Leland, E. S.; Baker, J.; Carleton, E.; Reilly, E.; Lai, E.; Otis, B.; Rabaey, J. M.; Wright, P. K.; Sundararajan, V. Improving Power Output for Vibration-Based Energy Scavengers. *IEEE Pervas. Comput.* **2005**, *4*, 28–36.
7. Hu, Y. F.; Zhang, Y.; Xu, C.; Lin, L.; Snyder, R. L.; Wang, Z. L. Self-Powered System with Wireless Data Transmission. *Nano Lett.* **2011**, *11*, 2572–2577.
8. Zhu, G.; Wang, A. C.; Liu, Y.; Zhou, Y. S.; Wang, Z. L. Functional Electrical Stimulation by Nanogenerator with 58 V Output Voltage. *Nano Lett.* **2012**, *12*, 3086–3090.
9. Wang, Z. L.; Song, J. H. Piezoelectric Nanogenerators Based on Zinc Oxide Nanowire Arrays. *Science* **2006**, *312*, 242–246.
10. Fan, F. R.; Tian, Z. Q.; Wang, Z. L. Flexible Triboelectric Generator. *Nano Energy* **2012**, *1*, 328–334.
11. Fan, F. R.; Lin, L.; Zhu, G.; Wu, W. Z.; Zhang, R.; Wang, Z. L. Transparent Triboelectric Nanogenerators and Self-Powered Pressure Sensors Based on Micropatterned Plastic Films. *Nano Lett.* **2012**, *12*, 3109–3114.
12. Zhu, G.; Pan, C. F.; Guo, W. X.; Chen, C. Y.; Zhou, Y. S.; Yu, R. M.; Wang, Z. L. Triboelectric-Generator-Driven Pulse Electrodeposition for Micropatterning. *Nano Lett.* **2012**, *12*, 4960–4965.
13. Wang, S. H.; Lin, L.; Wang, Z. L. Nanoscale Triboelectric-Effect-Enabled Energy Conversion for Sustainably Powering Portable Electronics. *Nano Lett.* **2012**, *12*, 6339–6346.
14. Zhu, G.; Chen, J.; Liu, Y.; Bai, P.; Zhou, Y. S.; Jing, Q. S.; Pan, C. F.; Wang, Z. L. Linear-Grating Triboelectric Generator Based on Sliding Electrification. *Nano Lett.* **2013**, *13*, 2282–2289.
15. Castle, G. S. P. Contact Charging between Insulators. *J. Electrostat.* **1997**, *40−1*, 13–20.
16. Niu, S. M.; Wang, S. H.; Lin, L.; Liu, Y.; Zhou, Y. S.; Hu, Y. F.; Wang, Z. L. Theoretical Study of the Contact-Mode Triboelectric Nanogenerators as Effective Power Source. *Energy Environ. Sci.* **2013**just accepted.
17. Liu, H. C.; Lee, C. K.; Kobayashi, T.; Tay, C. J.; Quan, C. G. Investigation of a MEMS Piezoelectric Energy Harvester System with a Frequency-Widened-Bandwidth Mechanism Introduced by Mechanical Stoppers. *Smart Mater. Struct.* **2012**, 21.
18. Rastegar, J.; Murray, R. Novel Two-Stage Piezoelectric-Based Electrical Energy Generators for Low and Variable Speed Rotary Machinery. *Act. Passive Smart Struct. Integr. Syst. 2010, Pts 1 and 2* **2010**, 7643.
19. Salter, S. H. Wave Power. *Nature* **1974**, *249*, 720–724.
20. Muetze, A.; Vining, J. G. Ocean Wave Energy Conversion - A Survey. *IEEE Ind Appl. Soc.* **2006**, 1410–1417.
21. Scruggs, J.; Jacob, P. Harvesting Ocean Wave Energy. *Science* **2009**, *324*, 1143–1143.